Measurement Report: An investigation of the spatiotemporal variability of aerosol in the mountainous terrain of the Upper Colorado River Basin from SAIL-Net

Leah D. Gibson[1,a], Ezra J.T. Levin[1,b], Ethan Emerson[1,c], Nick Good[2,d], Anna Hodshire[1,b], Gavin McMeeking[1,d], Kate Patterson[1,a], Bryan Rainwater[1,b], Tom Ramin[1,d], and Ben Swanson[1,d]

[1]Handix Scientific, Fort Collins, CO, USA
[2]Good Science, Fort Collins, CO, USA
[a]now at: Colorado Department of Public Health and Environment, Denver, CO, USA
[b]now at: METEC Research Group, Colorado State University Energy Institute, Fort Collins, CO, USA
[c]now at: Sonoma Technology, Petaluma, CA, USA
[d]now at: CloudSci, Fort Collins, CO

Correspondence: Leah D. Gibson (lgibson@handixscientific.com)

Abstract. In the Western US and similar topographic regions across the world, precipitation in the mountains is crucial to the local and downstream freshwater supply. Atmospheric aerosols can impact clouds and precipitation by acting as cloud condensation nuclei (CCN) and ice nucleating particles (INP). Previous studies suggest there is increased aerosol variability in these regions due to the complex terrain, but none have quantified the extent of this variability. In fall 2021, Handix Scientific contributed to the US Department of Energy (DOE)-funded Surface Atmosphere Integrated field Laboratory (SAIL) in the East River Watershed (ERW), CO, USA by deploying SAIL-Net, a novel network of six aerosol measurement nodes spanning the horizontal and vertical domains of SAIL. The ERW is a topographically diverse region where single measurement sites can miss important observations of aerosol-cloud interactions. Each measurement node included a small particle counter (POPS); a miniature CCN counter (CloudPuck); and a filter sampler (TRAPS) for INP analysis. SAIL-Net studied the spatiotemporal variability of aerosols and the usefulness of dense measurement networks in complex terrain. After the project's completion in summer 2023, we analyzed the data to explore these topics. We found increased variability compared to a similar study over flat land. This variability was correlated with the elevation of the sites, and the extent of the variability changed seasonally. These data and analysis stand as a valuable resource for continued research into the role of aerosols in the hydrologic cycle and as the foundation for the design of measurement networks in complex terrain.

1 Introduction

In mountainous regions, winter snowpack and overall precipitation are vital for maintaining local and downstream freshwater supplies. In these areas, atmospheric aerosols play a role in local precipitation patterns, acting as cloud condensation nuclei (CCN) and ice nucleating particles (INP) (Jirak and Cotton, 2006; Lynn et al., 2007). It is therefore critical to understand and monitor aerosol concentrations in these areas. Ambient aerosols are spatially and temporally complex due to their many sources

and relatively short atmospheric lifetimes (Anderson et al., 2003; Weigum et al., 2016). This complexity is further amplified in mountainous terrain (Zieger et al., 2012; Yuan et al., 2020; Nakata et al., 2021). Direct measurements of aerosols across spatial and temporal scales are therefore essential to fully understand the role of aerosols in cloud formation and precipitation.

Orographic clouds created by topographically forced upward motion are an important contributor to winter snow in mountainous regions. In these clouds, ice crystals form in the upper layers and then fall through a supercooled liquid layer, collecting rime and growing larger before reaching the ground as snow or graupel. This process is sensitive to the amount of CCN and INP present (Creamean et al., 2013; Levin et al., 2019). The amount of riming gathered by descending crystals is contingent upon the size of supercooled liquid droplets, where smaller droplets are less efficiently collected. In CCN-rich clouds, droplets are smaller, resulting in reduced rime and overall precipitation. In the Rocky Mountains of Colorado, Saleeby et al. (2011) found that decreased riming causes a shift in precipitations from windward to leeward slopes and potentially into different watersheds. The riming process is also oppositely influenced by INP, where higher concentrations of INP increase precipitation (Rosenfeld et al., 2014). Thus, understanding the spatial and temporal variability of atmospheric aerosols is necessary to understand the role of aerosols in the hydrologic cycle in mountainous regions and the subsequent impacts on freshwater availability.

To further study land-atmosphere interactions and their impact on the hydrologic cycle in mountainous regions, the US Department of Energy (DOE) supported the Surface Atmosphere Integrated field Laboratory (SAIL) in the East River Watershed (ERW) of the Upper Colorado River Basin in southwestern Colorado. The Colorado River Basin covers parts of Colorado, Utah, Nevada, New Mexico, California, and all of Arizona. These states withdraw an average of 17 million acre-feet of water each year (Maupin et al., 2018). In the past 20 years, the basin has experienced increasingly intense droughts, leading to concern over freshwater availability in the Western United States. Precipitation is affected by anthropogenic aerosols, and it is estimated that the Colorado River Basin loses approximately 538,0000 acre-feet of water each year due to an increase in CCN caused by anthropogenic emissions (Jha et al., 2021). Thus, one of the main goals of the SAIL campaign was to improve earth system modeling to better predict the timing and availability of water resources from the mountains in this region.

Two monitoring sites were deployed in the East River Watershed from fall 2021 to spring 2023 as part of SAIL. The two sites were the Aerosol Observation System (AOS) located on Crested Butte Ski Mountain, and the ARM Mobile Facility (AMF-2), located at the Rocky Mountain Biological Laboratory in Gothic, Colorado. Both sites collected a variety of aerosol and atmospheric measurements (Feldman et al., 2023). While these two sites provided comprehensive aerosol measurements, they may not have fully represented the complete spatial variability of aerosol concentrations due to the complex terrain of the region (Schutgens et al., 2017). Thus, additional measurement locations were beneficial, if not crucial, to understanding aerosol-cloud interactions in complex terrain.

To gain a more comprehensive understanding of aerosols in the region, we deployed SAIL-Net, a distributed network of six measurement nodes spanning the domain of the SAIL research area from October 2021 to July 2023. Each node measured aerosol particles between 140 nm and 3.4 μm in diameter using a small particle counter (POPS, (Gao et al., 2016)), CCN using a miniature CCN counter (CloudPuck), and INP using the Time-Resolved Aerosol Filter Sampler (TRAPS, Creamean et al. (2018)). Our approach was similar to other studies that aimed to better characterize and understand aerosols and gas-phase pollutants using networks of lower-cost sensors (Caubel et al., 2019; Kelly et al., 2021; Asher et al., 2022). Such studies have

identified neighborhood-level variations in pollutant concentrations (Schneider et al., 2017; Popoola et al., 2018; Caubel et al., 2019). Small-scale variations such as this are poorly represented in models and poorly measured by a single monitoring system (Caubel et al., 2019). Previous work has shown the representation error (the ability of measurements to represent a larger area) increases with complex orography, leading to decreases in model accuracy (Schutgens et al., 2017). The overall goal of SAIL-Net was to improve our understanding of the variability of aerosol in the ERW, thus increasing our knowledge of aerosol-cloud interactions in this region and informing the usefulness of distributed networks of measurements for future studies. We met this goal by answering the following science questions:

1. **What is the aerosol temporal variability, and how does aerosol inhomogeneity vary seasonally?** Is there significant seasonal variability in sources, or are short-term meteorological conditions the most important determining factor in sources for cloud nuclei?
2. **What is the aerosol spatial variability?** What are the aerosol characteristics at cloud base, presumably the particles most representative of those acting as cloud nuclei?
3. **How should measurement networks be designed to capture aerosol-cloud interactions, and what do they need to measure?** Can a single measurement site accurately represent aerosol properties in regions of complex terrain?

The goal of this paper is to introduce SAIL-Net, highlight initial observations of the POPS data, and use these findings to address the science questions. We hope these data and analyses inspire future research in studying the variability and impact of aerosol in mountainous terrain.

Section 2 of this paper introduces the instrumentation, sites, and data of SAIL-Net. Next, Sect. 3 uses the data from the POPS to address our scientific questions and highlights the trends we have seen in the data. This is broken into three subsections. First, Sect. 3.1 identifies the temporal variability of aerosol in the ERW by looking at seasonal and diurnal patterns. Next, Sect. 3.2 highlights the variability of aerosol in the region and suggests conditions and sources that may affect this variability. Lastly, in Sect. 3.3, we compare the network as a whole to determine if a single measurement site could sufficiently represent the ERW.

2 Methods

Each site included a suite of three relatively low-cost, lightweight microphysics instruments manufactured by Handix Scientific to measure aerosol size distributions (POPS), CCN concentrations (CloudPuck), and INP concentrations (TRAPS). Together this network of instruments formed a comprehensive picture of aerosol-cloud interactions in the region. These instruments were chosen because their size, price, low power requirements, and self-sufficiency were the optimal combination to support a distributed network of sites in remote terrain.

The three instruments were secured inside a weatherproof enclosure and mounted on 3 meter tall scaffolding to keep the instruments above the snow in the winter. The inlets of the instruments faced downward and were protected by a baffle. Four of the six sites ran on solar power while the other two sites used established ground power sources.

This manuscript will focus on data from the Portable Optical Particle Spectrometer (POPS). The POPS is a small, low-cost optical particle counter initially developed at NOAA by Gao et al. (2016) and commercialized by Handix Scientific. In the last few years, it has been recognized for its accuracy and reliability as a low-cost sensor, and used in a number of field deployments and campaigns (Mei et al., 2020; Brus et al., 2021; Asher et al., 2022; Todt et al., 2023). The instrument measures the intensity of light scattered by particles passing through a 405 nm laser to optically size particles into user-selectable size bins between approximately 140 nm and 3.4 μm, and measures at a one-second resolution.

The POPS operated continuously at each SAIL-Net node, except during power outages, deep snows that temporarily buried some inlets, or other instrument malfunctions. This was the largest and longest dataset produced during SAIL-Net.

2.1 Network description

SAIL-Net consisted of six measurement nodes spread across the ERW near Crested Butte, CO. The primary objective in site placement was to select locations that captured the vertical variation in aerosol properties while also spanning the domain of the SAIL campaign. The elevation of the sites ranged from roughly 2750 m along the valley floor of the ERW to approximately 3500 m near the top of Crested Butte Mountain, which is one of the taller peaks in the ERW. The farthest distance between sites was 14 km, while the closest two sites were approximately 1 km apart. The disparate elevations of the sites resulted in different vegetation surrounding the sites. Table 1 describes each site. A map of the sites is also provided in Fig. 1, and Fig. 2 provides a photo of each site.

2.2 Data acquisition and post-correction

SAIL-Net sites were visited approximately monthly. During each visit, a suite of checks was performed to ensure instrument reliability and to document instrument drift. The POPS underwent the most checks and monitoring. We checked the inlet flow of the instrument and recorded the accuracy of the POPS in sizing 500 nm aerosolized polystyrene latex beads (PSL check). This information was used to later post-correct the data. We did not recalibrate the POPS in the field to correct drift at any point during the campaign in order to avoid causing discontinuities in the raw data. However, if any of the instruments required major repairs, it was removed, repaired, or replaced, and returned the following month. When a new or repaired POPS was returned to the field, its sizing had been recalibrated. In these cases, there was some discontinuity in sizing accuracy, but these were corrected in the post-analysis data as discussed below.

The data collected by the POPS during SAIL-Net were binned into one of 16 bins as number counts based on the measured size of the particle. These number counts were converted to number concentrations in publically available datasets (Gibson and Levin, 2023). In diameter space, the widths of the bins are not equal but increase non-monotonically with size. The size range of particles for smaller bins is approximately 15 nm, while the size range for larger bins is approximately 600 nm. The following description will provide insight into why the bins are unequal widths in diameter space and why this increase is not strictly monotonic.

The data correction process focused on correcting drift in the POPS sizing accuracy. All POPS instruments in SAIL-Net experienced some drift, but the drift rate and amount were not uniform across the different instruments. We collected data from

Site Name	Location	Elevation	Deployment Months	Description
Pumphouse	38.9211°N, 106.9495°W	2765 m	Oct. 2021–July 2023	Instrumentation was mounted on scaffolding and ran on solar power. Located in a meadow next to the East River in the East River Valley.
Gothic	38.9561°N, 106.9858°W	2918 m	Oct. 2021–July 2023	Colocated with AMF-2 in a meadow near Gothic, also in the East River Valley. Instrumentation was mounted on scaffolding and ran on ground power. Higher traffic and human activity nearby in the summer.
CBMid	38.8983°N, 106.9431°W	3137 m	Oct. 2021–June 2023	Colocated with AOS on Crested Butte Ski Resort. Instrumentation was mounted on AOS trailer and ran on ground power. Near a groomed ski run in the winter.
Irwin	38.8874°N, 107.1087°W	3177 m	Oct. 2021–July 2023	Instrumentation was mounted on scaffolding and ran on solar power. Located in an evergreen forest near a snowcat barn and snowmobile road, which was active in the winter.
Snodgrass	38.9271°N, 106.9905°W	3333 m	Oct. 2021–July 2023	Instrumentation was mounted on scaffolding and ran on solar power. Remote, off-trail location on the side of Snodgrass Mountain, but directly north of Crested Butte town.
CBTop	38.8888°N, 106.9450°W	3482 m	June 2022–July2023	Instrumentation was mounted on shared tower and ran on solar power. Located near the top of Crested Butte Ski Resort.

Table 1. Location and brief site descriptions for the six SAIL-Net sites in the East River Watershed.

PSL checks for the majority of site visits, but not all. Some sites were not visited during certain months due to accessibility issues, or the PSL check was not performed due to instrument malfunctions or weather. Thus, some assumptions were made during post-correcting to account for these gaps. We assumed the POPS were performing at their factory calibration level at the start of the measurement period in fall 2021 (or summer 2022 in the case of CBTop), and therefore did not need post-correction until drift was observed by the PSL check. We also assumed that the PSL checks were representative of an entire month. Lastly, if a month missed a PSL check, we assumed the drift was linear to allow interpolation between missing PSL checks.

The post-correction process involved shifting the boundaries of bins to size 500 nm PSL in the correct bin at the completion of the data correction process. A POPS experiences drift for two primary reasons: either the laser diode loses intensity over time or the mirror that reflects light becomes dirty. In either case, the lower intensity of light causes particles to be sized smaller than their true size, and thus the drift of the POPS is monotonically decreasing over time. The bin that contains 500 nn sized particles has a lower bound of 497 nm. Thus, the drift in a POPS is caught early on because 500 nm sized particles will very quickly be sized into the bin below as the drift starts to occur.

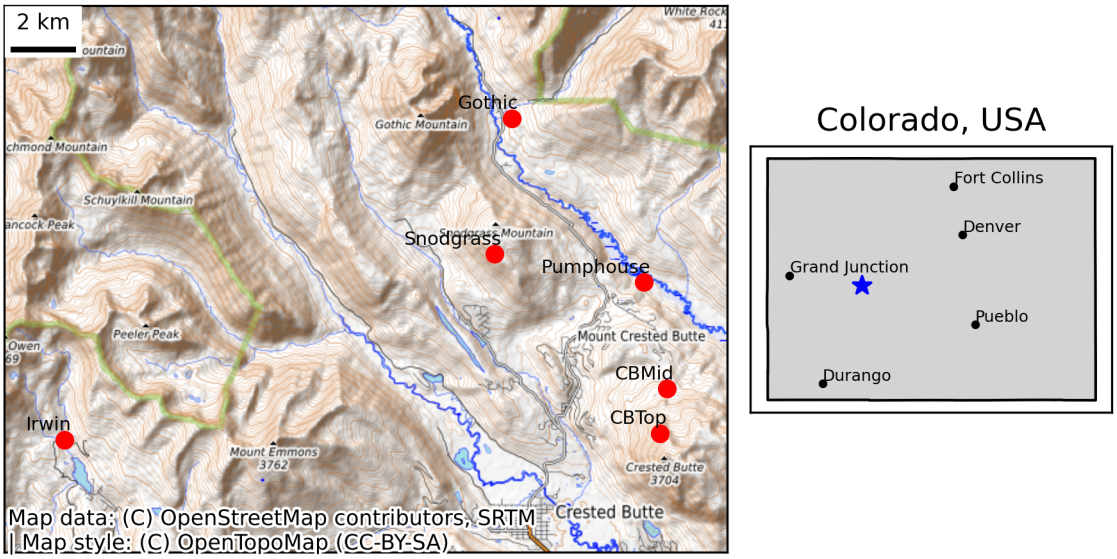

Figure 1. The figure on the right shows a map of the state of Colorado, USA. The region where SAIL-Net measured is marked with a blue star. The plot on the left shows a zoomed in topographic map of this region where the six sites in SAIL-Net are marked with a red dot. The network spanned approximately 8 km vertically (North-South) 14 km horizontally (East-West), and covered approximately 750 m of elevation difference. ©OpenStreetMap contributors 2024. Distributed under the Open Data Commons Open Database License (ODbL) v1.0.

As a particle passes through the beam of the laser diode, the light is scattered and the digitizer in the POPS reads the raw signal of the light intensity. The sizing range of the POPS is determined by taking the base 10 logarithm of the range of the digitizer. In logarithmic space, the range is 1.75 to 4.806. The bins of the POPS are then determined by dividing this range into n bins of equal width w, where

$$w = (4.806 - 1.75)/n. \tag{1}$$

These log values are converted to diameter space using Mie theory. In diameter space, the bins are no longer equal in width.

The intuition for the post-correction comes from considering the raw signals that the digitizer would receive and scaling the signal to properly bin it. The following explanation shows that this is equivalent to simply shifting the current bins of the POPS. When the POPS sizes particles accurately, 500 nm PSL should be placed into the bin containing 500 nm sized particles. Let the midpoint of this bin in logarithmic space be called x. Suppose 500 nm PSL is instead sized into a different bin with midpoint y in logarithmic space. Thus, the digitizer saw a raw signal of 10^y instead of 10^x. To correct for this error, we would need to scale all raw signals by $10^x/10^y$. Since this is a post-correction and all raw signals have already been received, we instead scale all digitizer bin boundaries by $10^x/10^y$ so that the drifted signals would be binned properly. The bin boundaries, b_i are defined in logarithmic space using the range of the digitizer and Eq. 1, but can be converted to raw signal using 10^{b_i}. Thus, to account for the drift, we apply a shift to all bin boundaries: $10^{b_i}(10^x/10^y)$. To then convert the raw signal back into logarithmic space,

Figure 2. Photos of the six sites in SAIL-Net. From left to right, top to bottom, the sites are Pumphouse, Snodgrass CBMid, Irwin, CBTop, and Gothic. Four of the sites ran on solar power, and the solar panels can be seen in the photos. CBMid and Gothic both ran on ground power.

which is necessary for converting back to diameter space, we take the base 10 logarithm of the raw boundaries:

$$\log_{10}(10^{b_i}(10^x/10^y)) = b_i + (x - y). \tag{2}$$

Since x and y are the midpoints of *equal* sized bins in logspace, $(x - y)$ is equivalent to the width of a bin, w, multiplied by the number of bins apart they are, m. Thus, the post-correction ends up being as simple as shifting all bins up by m spaces, keeping bin boundaries the same, until 500 nm PSL, and all particles, are sized correctly.

As an example, if the PSL check sized 500 nm particles into one bin smaller, then the post-correction process would move all particles from bin one into bin two, bin two into bin three, and so on. Then the particles that were previously sized as 143 nm to 155 nm in bin one would now be sized as 155 nm to 170 nm, adopting the size range of bin two. Because of this upward shifting, the lowest size that the POPS measured increased throughout the deployment. For the majority of the following analysis, the minimum particle size used will be 170 nm instead of the 140 nm that is standard with the POPS to account for this shift.

Once data were rebinned, additional smoothing was performed by computing one minute rolling averages of the data to remove excessive noise. These post-corrected and cleaned data were used for all analysis described in the following section. All time series plots and analysis use UTC timestamps unless otherwise noted. Figure 3 displays the completeness of 170

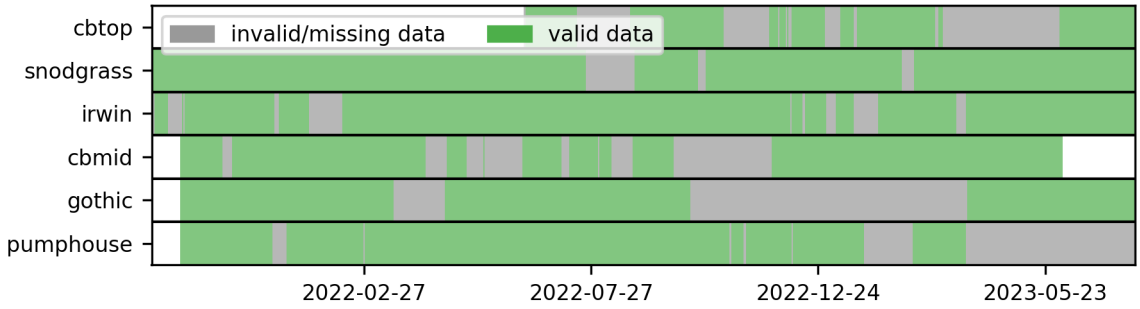

Figure 3. The completeness of 170 nm to 3.4 μm POPS data for each day. Each day marked "invalid/missing data" indicate times that the site was in place but no data was recorded, or the data did not meet quality assurance standards. The days marked "valid data" indicate days that the site has valid data. The white space indicates times that the site was not yet or no longer in place. The percent of valid data for each site is: cbtop: 60%; snodgrass: 92%; irwin; 88%; cbmid: 76%; gothic: 66%; and pumphouse: 75%.

nm to 3.4 μm size particle data for each site in the network. We assume that the post-correction process has removed any instrument caused variation between different POPS, and therefore, the remaining variability observed in the data is due to environmental conditions. These cleaned POPS data, raw POPS data, and CloudPuck data are all publically available on the ARM Data Discovery (Gibson and Levin, 2023). INP data will become available once the filters have been analyzed by Perkins et al. (2023).

3 Results and discussion

This section uses data from the six POPS to address the science questions proposed in the Introduction. The POPS produced the longest and highest temporal resolution dataset, which allows the study of spatiotemporal variability in aerosol concentrations and distributions. Figure 4 displays the complete time series of 170 nm to 3.4 μm sized aerosol concentration data from the POPS at the six sites. The data are averaged daily by UTC.

The daily averaged data indicate that all the sites exhibited similar daily behavior and seasonal trends. The sites experienced higher total aerosol concentrations in the summer and lower in the winter, which was consistent with the seasonal trends of other mountainous regions (Gallagher et al., 2011). Concentrations peaked in the late summer and reached a minimum in January. However, the maximum recorded concentration occurred on 13 June 2022, at Gothic, with an average daily concentration of 672 cm^{-3} due to smoke from the Flagstaff wildfires burning in Arizona. Concentrations were again abnormally high in September 2022 due to biomass burning as well. The unique differences and trends in the data are discussed below and broken into three sections based on the science questions posed in the Introduction.

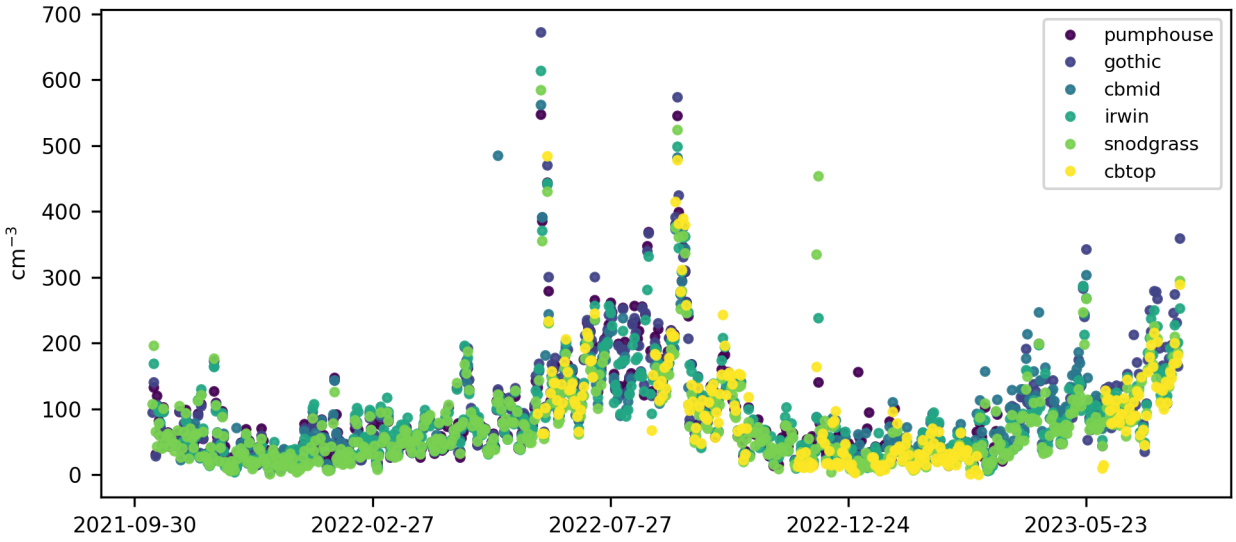

Figure 4. The time series of daily averaged concentration of 170 nm to 3.4 μm sized aerosol for the six sites in SAIL-Net.

3.1 Seasonality and diurnal patterns

Both seasonal and diurnal cycles were observed in the POPS data. In this section, we use the time series of the network mean of the data to study the temporal variability of aerosol. The network mean at time t, N_t, is the average of m sites' values at time t. Thus given a time series at each site; $\{x_{i,t=1}, x_{i,t=2}, \ldots, x_{i,t=n}\}$ where i is the site number, the network mean time series of m sites is

$$\{N_1, N_2, \ldots, N_n\} = \left\{ \frac{\sum_{i=1}^{m} x_{i,1}}{m}, \frac{\sum_{i=1}^{m} x_{i,2}}{m}, \ldots, \frac{\sum_{i=1}^{m} x_{i,n}}{m} \right\}. \tag{3}$$

Since the network mean takes an average of spatially dispersed sites, it removes much of the noise and variability caused by local sources or instrument drift and can be used as a proxy for a model grid cell in the region.

Most sites had gaps in data at some point, so when one or multiple sites were missing data, the network mean was computed from the sites with data. This choice was made to preserve as much temporal coverage as possible and attain a clear picture of seasonal trends. For further discussion of the network mean and its ability to represent the East River Watershed, see Sect. 3.3. In the following analysis, the sum of aerosol concentrations between 170 nm and 3.4 μm are used, unless otherwise specified.

SAIL-Net collected data during two very different winters. The 2022 snowpack in the Gunnison Basin, which the ERW is a part of, was close to the median for the region. However, if it were not for a large snow in late December 2021, the snowpack would have been well below normal. In contrast, the 2023 winter saw higher than normal snowfall, with snow water equivalent peaking in the 90th percentile of the 30-year median (NRCS, 2023). Despite the very different winters, the daily average aerosol

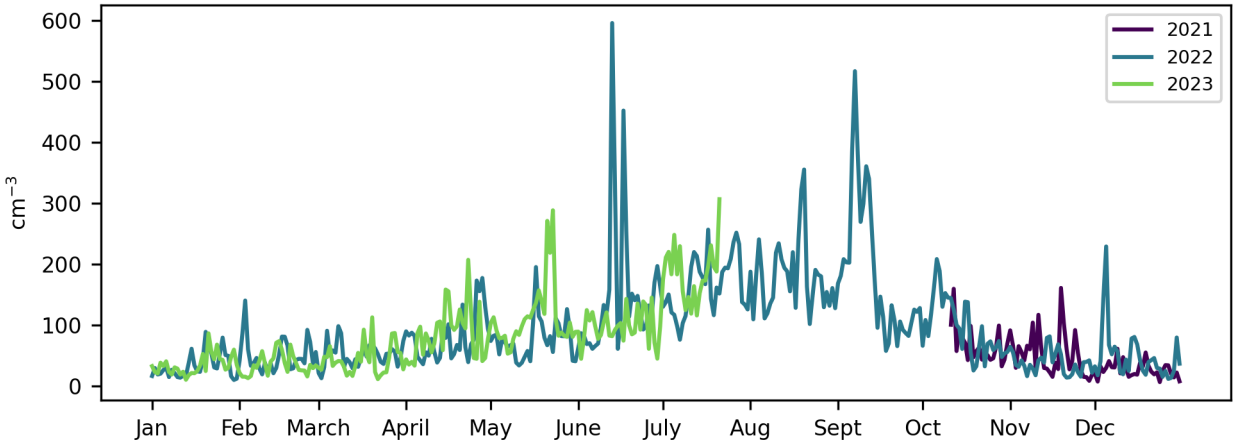

Figure 5. The network means of daily 170 nm to 3.4μm sized aerosol concentrations, overlaid by day of the year.

concentrations for 170 nm to 3.4 μm sized particles of the network mean had similarities over the years. Figure 5 displays the network means overlaid by day of the year. The main difference between the two years occurred on and in the few days after 13 June 2022, when the spikes in concentration were due to smoke from the Flagstaff wildfires in Arizona. The maximum recorded concentration occurred during this time. The minimum recorded concentration of the network mean occurred on 24 December 2021, with a concentration of 7 cm^{-3}. This minimum was likely caused by scavenging from heavy snow that fell on the same date. Below, we further analyze the temporal trends in aerosol data.

The distribution of particle sizes changed monthly and also slightly differed between the two years, depending on the month. Figure 6 displays the monthly average number size distribution (N vs D_p) of aerosol overlaid by month. In general, supermicron concentrations peaked in April and were higher in March through June, primarily due to aeolian dust transported from the desert southwest (Skiles et al., 2015). The two spring dust seasons were noticeably different, as seen by the differing shapes of the number size distribution for supermicron sized particles. According to the POPS data, supermicron concentrations increased in March and lasted through June 2022, whereas in 2023, April saw the highest supermicron concentrations. Submicron concentrations peaked in the summer and quickly dropped off in the fall.

Figure 7 plots the time series of daily averaged particle size distributions for the entire measurement period. Here, we see the seasonality in different particle sizes. Particles between 140 and 300 nm increased in the spring and early summer and peaked in late summer. There was a period in both winters around late December and early January when the air was extremely clean, and there were very few particles larger than approximately 300 nm. This figure also provides another look into the spring dust events, which were characterized by higher than normal concentrations of supermicron-sized particles.

The diurnal cycles in aerosol concentrations changed seasonally and varied between sites. Figure 8 plots the average diurnal cycle of 170 nm to 3.4 μm sized aerosol concentrations for each SAIL-Net site seasonally. Concentrations were averaged hourly and then grouped by meteorological season. The shaded region around each line displays the interquartile range of the

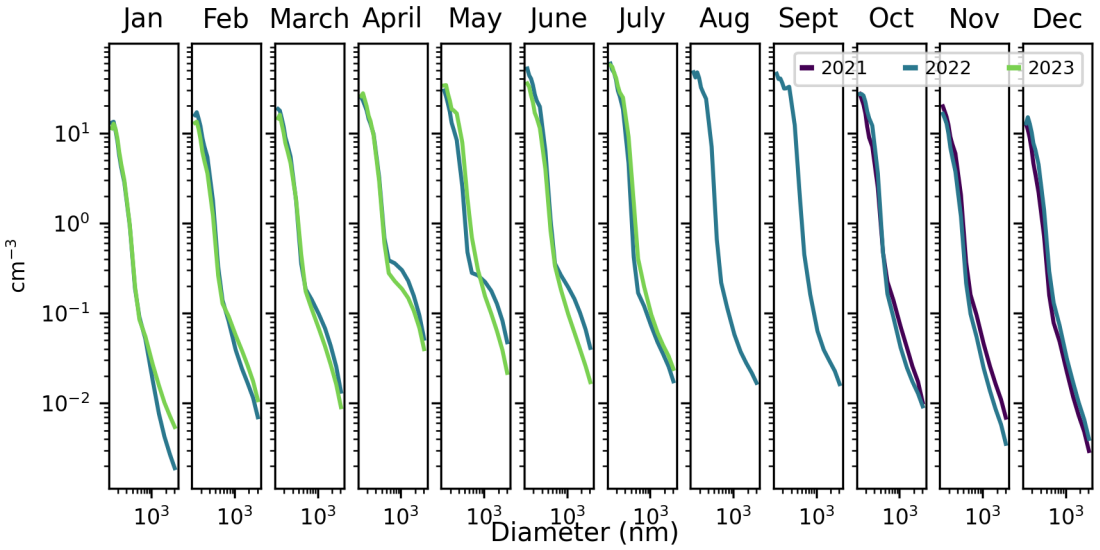

Figure 6. The number size distribution of the network mean is averaged monthly. When multiple years of data are present, both are plotted. These plots used the full 140 nm to 3.4 μm size range of the POPS.

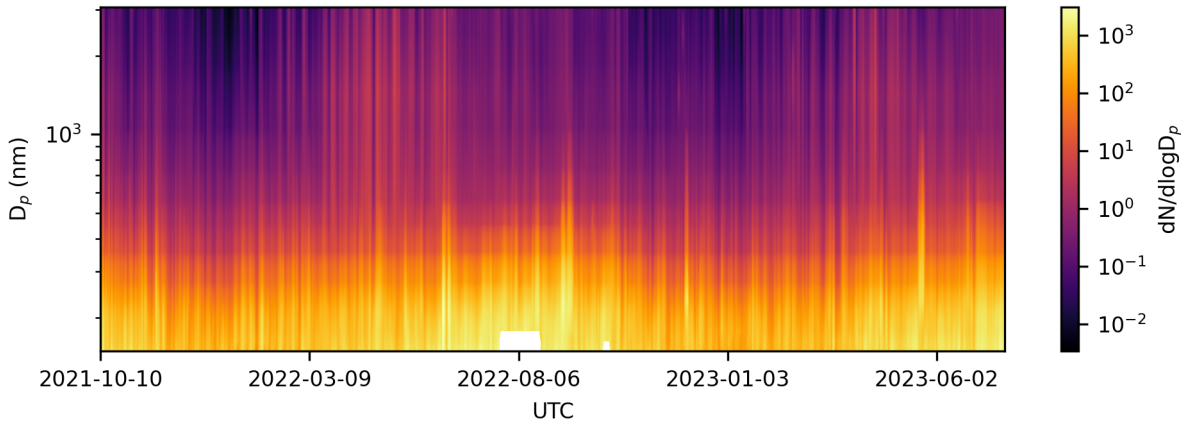

Figure 7. The time series of the measured particle size distributions of the network mean. Data were averaged daily. This plot uses the full 140 nm to 3.4 μm size range of the POPS.

seasonal data. For this analysis, we removed data from 13 June 2022 to 16 June 2022 so that the abnormally high concentrations caused by wildfire smoke would not affect the trend.

The diurnal cycles were most pronounced in the summer and fall when there were higher total aerosol concentrations. In contrast, there were minimal to no diurnal cycles observed in the winter and spring. The lack of diurnal cycles in the winter months could partially be attributed to less vertical mixing of the boundary layer throughout the day (Gallagher et al., 2011). Irwin does seem to have some patternicity in the winter and spring, with concentrations increasing in the afternoon, but we believe this increase was due to consistent snowcat and snowmobile activity around the site during these seasons.

While the diurnal cycles look different across the SAIL-Net sites, there was an underlying consistency in the daily trends in the summer and fall. Aerosol concentrations tended to increase overnight and into the morning and peaked in the early afternoon. Concentrations then decreased throughout the late afternoon and evening. This behavior was especially clear for Pumphouse and Gothic in the summer, possibly due to the influence of anthropogenic activities around the sites, or due to unique conditions in the East River Valley where both sites were located. These observations were partially consistent with the diurnal analysis from Gallagher et al. (2011) at Whistler Mountain, which studied the seasonal and diurnal patterns of CCN. They found that diurnal cycles were more distinct in warmer months and less so in the winter. They also observed increasing CCN concentrations from 08:00 until approximately 16:00 LST as a result of new particle formation (NPF). While this daytime increase was also observed in the SAIL-Net data, we were unable to determine if NPF was driving this increase since the POPS cannot measure small enough particles to observe this. Likely, the height of the convective boundary layer coupled with anthropogenic activities in the nearby town of Crested Butte was driving the nighttime to midday increases in aerosol concentrations. However, more analysis would be necessary to be certain.

3.2 Spatial variability

Networks of sensors are useful in cities and more polluted areas because aerosol concentrations vary dramatically over small spatial scales (Popoola et al., 2018; Caubel et al., 2019). In less populated areas such as the ERW, there are not as many local sources of emissions. However, aerosol properties can vary with elevation changes (Zieger et al., 2012). This section explores the spatial variability of the region and its relationship with elevation.

Figure 4 showed that all sites were reasonably similar on a daily timescale. However, there was still variability within the data, especially on a smaller timescale. Sub-daily variability was primarily due to local emissions and distances between sites. We were able to identify the sources of some of this variability, and a few examples are described below.

CBMid and Irwin experienced spikes in 155 nm to 300 nm sized particles from late November to early April, which we attributed to nearby snowcat and snowmobile activity. The top plot in Fig. 9 demonstrates this for a few days of Winter 2022. The spikes at CBMid occurred during the night local time, corresponding with Crested Butte Ski Resort's nightly grooming of their runs. The spikes at Irwin occurred roughly between 9 am and 3 pm local time, corresponding with the times that snowmobiling and other winter activities would take place. Concentrations at Gothic were influenced by increased anthropogenic activity in the summer. The middle plot of Fig. 9 displays these effects compared to Pumphouse, which was also in the East River Valley. The road to Gothic opened at the end of May 2022, aligning with the start of noisy spikes occurring at Gothic. It is unclear if

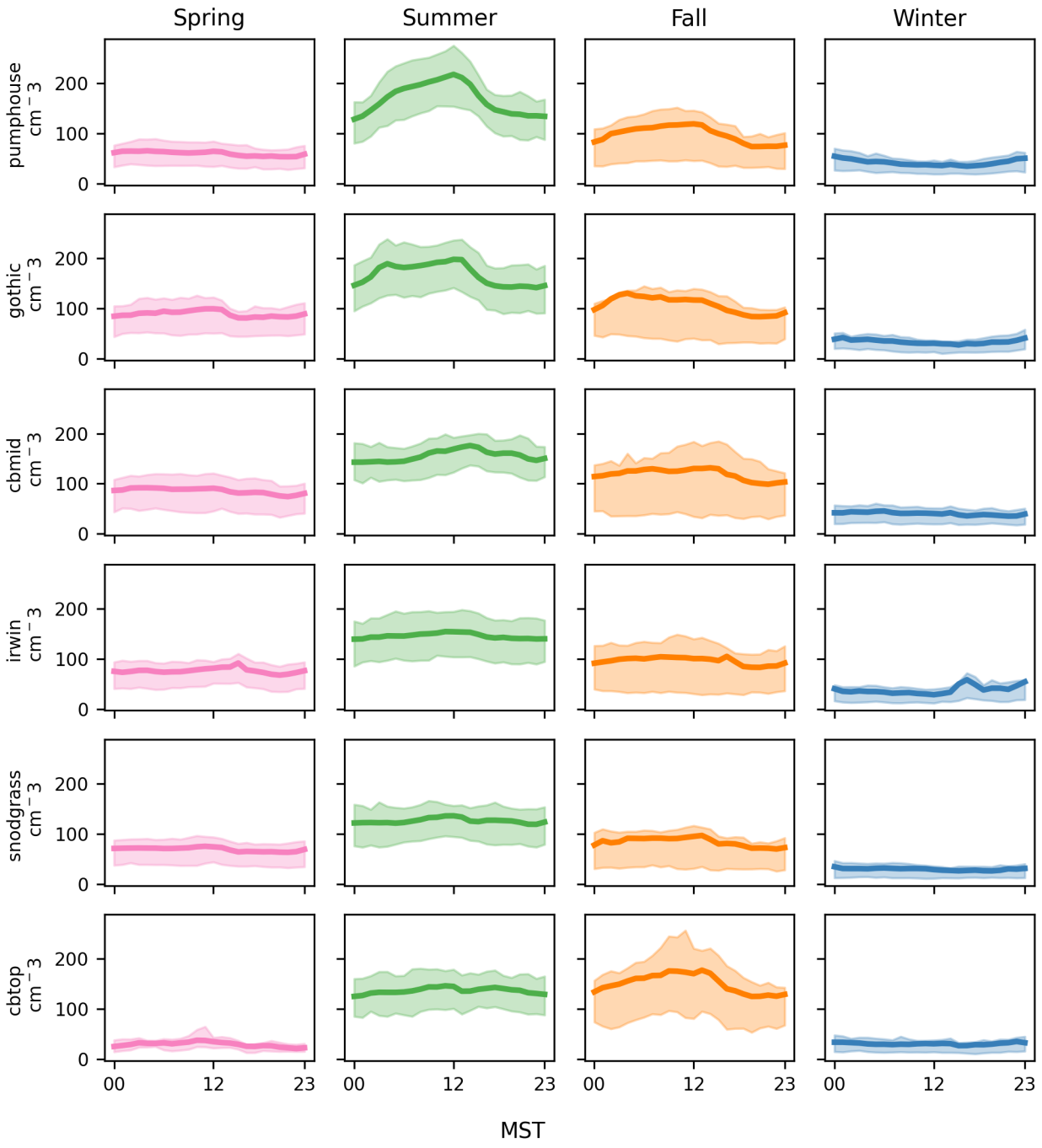

Figure 8. The daily diurnal cycle of hourly 170 nm to 3.4 μm sized aerosol concentration averaged seasonally for each SAIL-Net site. The shaded band around each line displays the interquartile range of the seasonal data. Times have been converted to Mountain Standard Time for ease of interpretation.

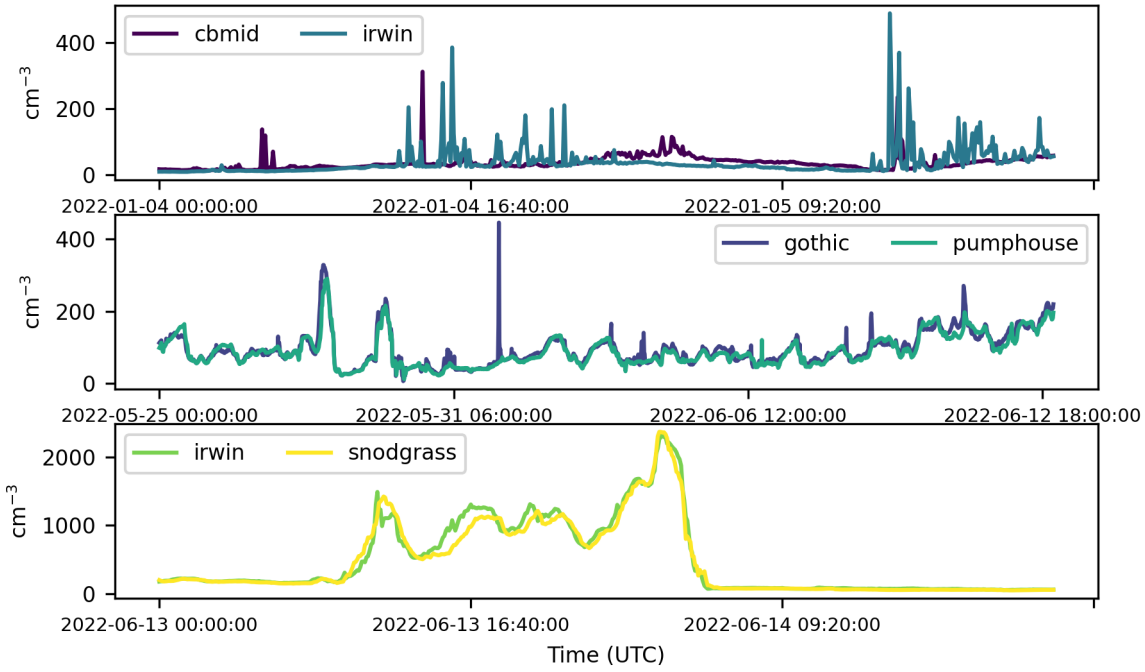

Figure 9. Examples of sub-daily variability among SAIL-Net. The top figure displays spikes in 155 nm-300 nm sized aerosol for CBMid and Irwin, which were both affected by winter snowsport activities. The middle plot displays noisy spikes at Gothic which began after Gothic road opened for the season. The bottom figure displays a lag in total aerosol concentration when a smoke plume moved into the region on 13 June 2022.

these spikes were due to road traffic or other activities near the town of Gothic, such as campfires. Variability between sites was also due to their dispersed locations. The bottom plot of Fig. 9 displays this behavior on 13 June 2022 when smoke from the Flagstaff Wildfires blew into the region. In this case, the sites report similar concentrations at a lag of one another, leading to increased variability as the plume moved into the area.

Beyond variability caused by local sources, we found that the variability between sites was partially influenced by their differences in elevation, supporting the findings from Zieger et al. (2012). Figure 10 plots the average pairwise percent difference in aerosol concentrations between two sites as a function of the elevation difference between the sites along the top row and the average pairwise percent difference as a function of the geographic distance between the sites on the bottom row. The percent difference was calculated daily as the absolute difference between the two sites divided by their average. These daily errors were then averaged over the total SAIL-Net deployment period to attain the plots in Fig 10. This was done for three groupings of particle sizes: 170 nm-300 nm, 300 nm-870 nm, and 870 nm-3.4 μm, and the full size range of 170 nm-3.4 μm.

These groupings were chosen based on the size ranges of particles that consistently had more similar concentrations. A linear regression was computed for each plot, and the Pearson correlation coefficient is reported at the top of each plot.

For the total size range and for the 170 nm to 300 nm size range, the most similar sites were Pumphouse and Gothic, with an average difference of 13.4%. Gothic and Pumphouse were both located in the East River Valley and were the two lowest elevation sites. The most different sites, CBTop and CBMid, were geographically the closest sites, with an average difference of 35%.

These plots reveal surprising results regarding the relationship between sites. The positive Pearson correlation values of 0.48 and 0.44 for the percent difference as a function of elevation difference for particles in the 170 nm to 300 nm range and for the full size range, respectively, indicate that sites closer in elevation have more similar concentrations. Thus, the variability between sites may partially be due to their differences in elevation.

We do not see a relationship of similarity for sites that are near one another. All Pearson correlation coefficients are negative when comparing percent difference as a function of difference between sites. This result indicates that the common assumption that spatially close data are more similar does not apply here, which is particularly surprising. However, this observed negative correlation may be an artifact of site placement. The SAIL-Net sites that were within 5 km of one another also differed approximately 300 m to 700 m in elevation and were thus more different. For the majority of SAIL-Net sites that were greater than 5 km apart, their elevations were typically within 350 m of one another, so concentrations were more similar. Thus, the positive relationship between measurement similarity and elevation may have negatively influenced the relationship between spatially proximal sites.

The variability across the sites also changed seasonally. The top plot of Fig. 11 plots the coefficient of variation (CV) across the sites over time. The CV represents the dispersion within a set of data. Using the daily average concentration of 170 nm to 3.4 μm sized particles at each site, the data were grouped by time, so that each time step provided a set of data across the sites for which to compute the CV. Each set was normalized using min-max scaling before computing the CV. This choice was made to account for the seasonality of the data while maintaining the relative distance between values. This figure also displays the monthly average CV overlaid on the daily CV.

Overall, there was fairly high variability across the sites. The average monthly CV was typically near or greater than one, indicating that the the standard deviation of sites' measurements was close to or larger than the mean of the data. There was less variability among the sites during the summer of 2022 than in other seasons. The variability also began trending downward as the weather warmed in 2023 but then increased in the last few weeks of deployment. We hypothesize that the increased variability in the cooler seasons could be partially due to the impact of snow-covered ground on the daytime convective boundary layer. Adler et al. (2023) saw a low convective boundary layer over snow-covered terrain in the East River Watershed and observed inversions at night. In some observations, the boundary layer was low enough that some high-elevation sites in SAIL-Net would be above the boundary layer, and thus measure different aerosol concentrations than below the boundary layer. However, another factor that likely affected the higher variability in the winter months was the low aerosol concentrations across the sites. The depths of winter experienced concentrations of less than 100 cm^{-3} on average. In these clean conditions, any local variability would amplify the differences between sites. The bottom plot of Fig. 11 displays the

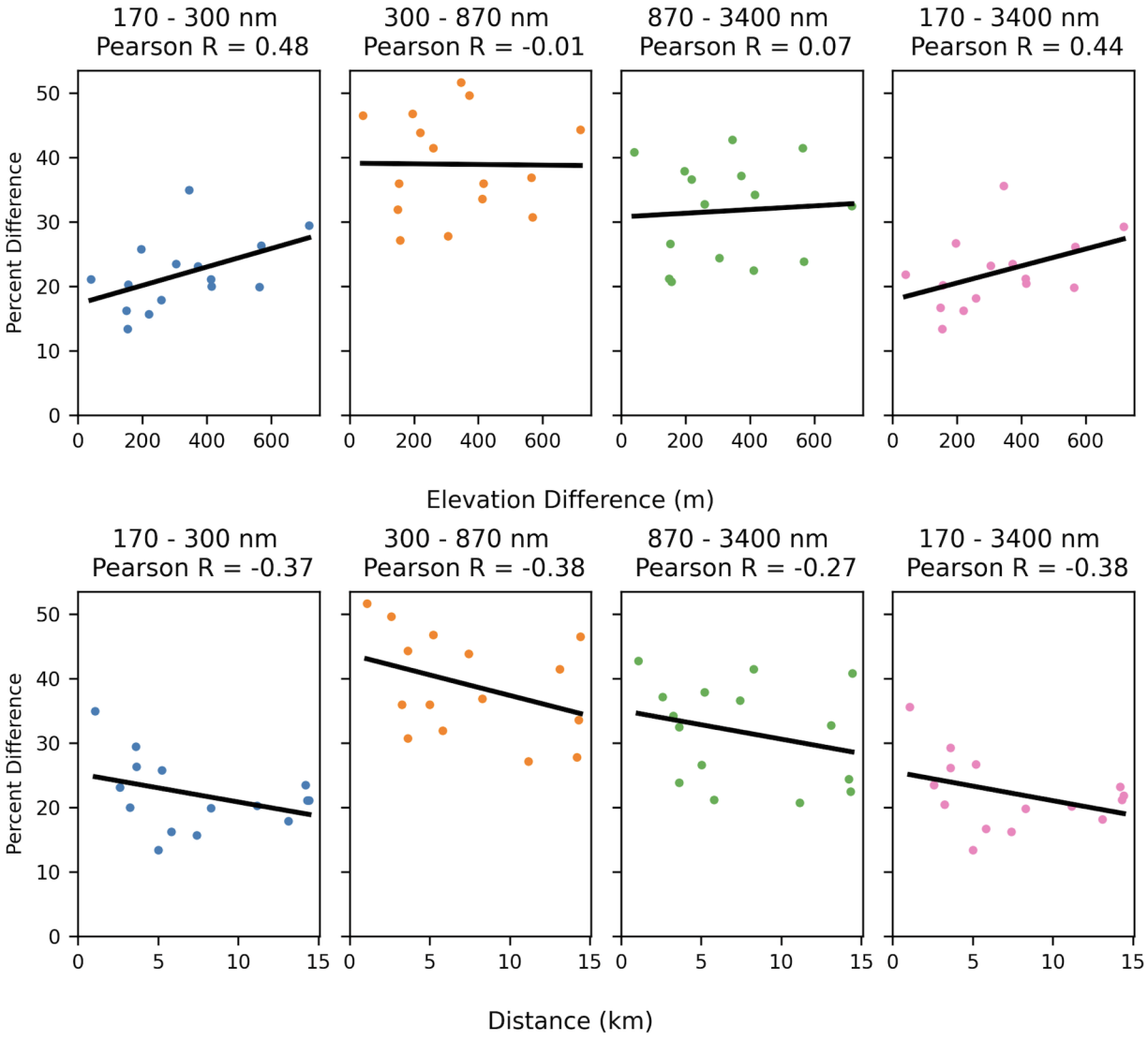

Figure 10. The top row of figures displays the average pairwise percent difference between sites as a function of the elevation difference between them. The bottom row again displays the average pairwise percent difference between sites, but this time as a function of the spatial distance between the sites. The average percent difference was computed from daily averages, and then averaged over the entire SAIL-Net deployment period.

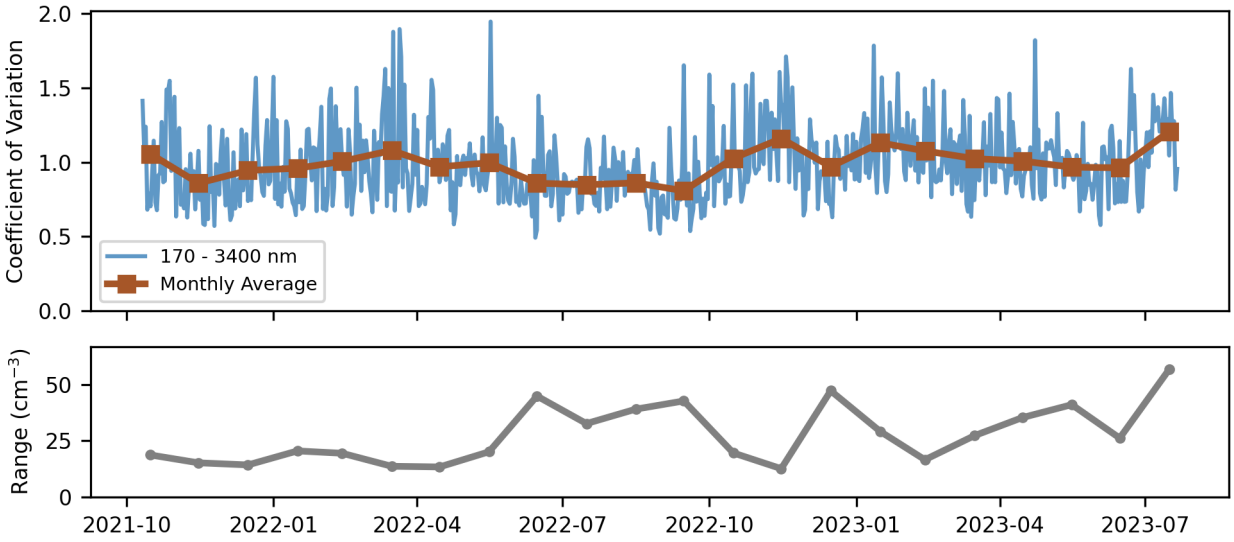

Figure 11. The time series of the coefficient of variation of daily averaged 170 nm-3.4 μm aerosol concentration for the SAIL-Net sites is plotted in blue in the top plot. The monthly average of the CV is plotted as brown squares overlaid on the daily CV. The bottom plot displays the average monthly range of concentrations between the sites.

monthly average range of concentrations between the sites, which was typically lower in the winter and higher in the summer. There appears to be an inverse relationship between the monthly averaged CV and the monthly averaged ranges, indicating that despite the min-max scaling applied to the data, the number counts of aerosol in different seasons affected the computed CV. Thus, although there appears to be higher variability in the colder months, this may predominantly be an artifact of the low wintertime concentrations.

3.3 Network representation

The previous subsections highlighted the temporal and spatial variability or aerosol in the ERW. We now use these data to investigate the optimal network design in the region and determine if a single site can accurately represent the aerosol properties of the region. This section is broken into two separate analyses. The first investigates the spatial representativeness of the sites, using a similar analysis approach to that of Asher et al. (2022) during POPSnet. The second analysis is more exploratory, and utilizes the varying altitudes of the SAIL-Net sites to compare ground-based measurements to airborne measurements from tethered balloon flights, which characterized the vertical column of air in the region.

3.3.1 Regional representation

As defined and studied by Schutgens et al. (2017), the representation error is the ability of a measurement to represent a larger area. There is often a significant difference between model estimates for a region and observed point measurements, leading to

inaccuracy (Schutgens et al., 2016). The representation error quantifies how similar each site is to the network mean (Eq. 3 in Sect. 3.1). Local sources affect measurements at a single site, so it can be advantageous to average over multiple sites to gain a more balanced picture of the region. However, if there are significant and consistent differences between sites, the network mean can masks this variability. The representation error treats the network mean as a proxy for the true regional value and then quantifies how different a single site is from the network mean. This provides meaningful insight into the usefulness of a network of sites in complex terrain by showing how different or similiar each site is to this proxy.

Using the equation from Asher et al. (2022), the representation error, e_t, is the normalized difference between a site observation and the network mean for an averaging period t

$$e_t = \frac{O_t - N_t}{N_t}. \tag{4}$$

During POPSnet in the Southern Great Plains, Asher et al. (2022) found the representation error decreased when data were averaged over longer periods. This was true for SAIL-Net as well. We used daily averaged data for the following analysis. The representation error was then computed for each site on every day when there was valid data. As with the computation of the network mean, not all days had data for all six sites, but in order to maximize the temporal span of data, we computed the representation error for sites whenever possible. Since the number of sites and number of days of data were not consistent across sites, this could have some effect on the results of the following analysis. However, we believe that given the approximately 600 sampling days, there was sufficient data that these missing values should not have a massive impact on the overall results.

Since the POPS data had significant seasonal changes with much higher concentrations in the summer than in the winter, we investigated the representation error seasonally. We grouped the daily representation errors by season, and Fig. 12 plots the results for three size ranges: the full 170 nm to 3.4 μm size range, 170 nm to 300 nm, and 300 nm to 3.4 μm. While the 300 nm to 3.4 μm size range has been broken apart in the analysis in the previous section, there were so few counts of particles larger than one micron that the representation errors were extremely high. In general, the representation error appeared higher in the winter and lower in the summer. However, the lower aerosol concentrations across the sites in the winter likely impacted the representation error, so caution must be used when comparing the errors across seasons.

Instead, we compared the representation errors across the sites within each season to determine the most representative site for each season and size range. The most representative site should have a median close to zero and a small range. In Fig. 12, the whiskers of the box plot bound the 5th and 95th percentiles. To determine the most representative site, we assigned a score to each site and size range by summing the median's absolute value and the data range between the 5th and 95th percentiles. Using this approach, the most representative sites for each size range were

- 170 nm to 3.4 μm: Pumphouse (Spring), Irwin (Summer), Gothic (Fall), Gothic (Winter),
- 170 nm to 300 nm: Pumphouse (Spring), Irwin (Summer), Gothic (Fall), Gothic (Winter),
- 300 nm to 3.4 μm: Pumphouse (Spring), Snodgrass (Summer), Pumphouse (Fall), CBTop (Winter).

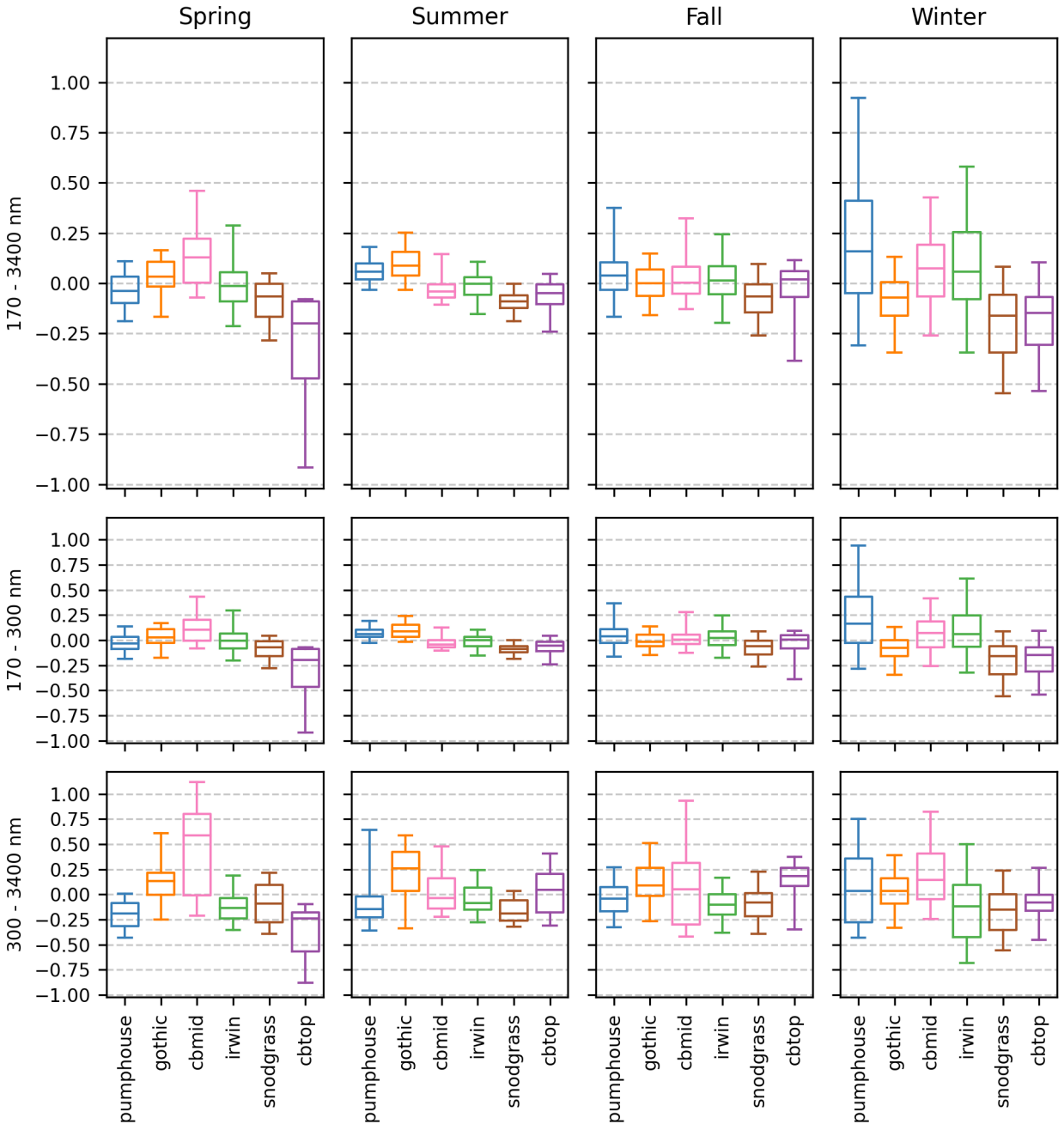

Figure 12. The representation error for each site broken apart by meteorological season and size ranges 170 nm-3.4 μm, 170-300 nm, and 300 nm-3.4 μm. The notches of each modified box plot indicate the following percentiles: 0.5, 0.25, 0.5 (median), 0.75, and 0.95.

The most representative site was inconsistent over different seasons and between the two size ranges. This suggests that the aerosol properties of the region are complex and vary across seasons and sizes and thus there is not one consistent most representative site for the region.

One of the observations driving the deployment of SAIL-Net was that aerosol complexity is increased in mountainous terrain compared to flat land (Zieger et al., 2012; Yuan et al., 2020; Nakata et al., 2021). The results of SAIL-Net further support this conclusion. In comparing the range of representation errors against the results of POPSnet (Asher et al., 2022), which collected data between October and March, SAIL-Net observed the same or higher errors across many of the sites in both the winter and spring. This suggests that aerosol complexity is increased in mountainous terrain since SAIL-Net sites were more spatially dense than POPSnet but still observed equal or greater error in the same season.

3.3.2 Vertical representation

The previous representation analysis quantified the ability of a single site to represent the larger area. Given the varying elevations of the sites, we also explored how representative the sites were of the vertical profile of air in the region. The six SAIL-Net sites were intentionally placed at various elevations across the ERW to span a portion of the altitudes in the area. To quantify how representative the SAIL-Net sites were of the vertical profile of aerosol in the region, we compared our data to the data collected during tethered balloon system (TBS) flights that took place in the ERW during the SAIL campaign (Mei et al., 2023). The TBS flights occurred at Gothic in 2022 and at Pumphouse in 2023. Each balloon was equipped with a POPS from Handix Scientific, which allowed for easy comparison with the POPS at the SAIl-Net sites.

During every TBS flight, the balloon was sent up vertically through the atmosphere. The balloon remained approximately in the same geographic location so that each flight generated a profile of the vertical air column in the region, where each measurement was associated with an altitude above sea level a_f and a time t_f. To compare the data from the TBS flight with SAIL-Net, we built a pseudo "vertical column" from the SAIL-Net sites. We did this by associating the altitude above sea level of each site, a_s with its measured total aerosol concentration at a time t_s, ignoring the geographical location of the site. Time t_s was determined by the time at which the altitude of the TBS balloon, passed within 2.5 m of the altitude above sea level of the site. Mathematically, t_s was the time at which $a_s - 2.5 < a_f < a_s + 2.5$. We then averaged the concentrations at site s in the one-minute window around t_s, and set this to be the value of the pseudo vertical column at the altitude, time pair (a_s, t_s). The error between the concentration reported by the POPS on the TBS flight and the concentration at the SAIL-Net site was computed for each (a_s, t_s) in the SAIL-Net vertical column.

We recognize the "vertical column" generated by the SAIL-Net sites is a crude approximation of a vertical column since it does not account for the differing geographic locations of the sites, and the measurements from the sites are ground-based instead of airborne. However, this approach provided a straightforward method for comparison between spatially dispersed ground-based measurements and airborne measurements. Figure 13 shows an example of TBS flight data plotted with the SAIL-Net vertical column for 13 and 14 June 2023. These two dates also highlight the variability in the vertical column of air over different flights. On some flights, like 13 June 2024, the column of air was well mixed, and concentrations at approximately 2800 m were within approximately 10 cm^{-3} of concentrations at nearly 3500 m. On other flights, like 14 June

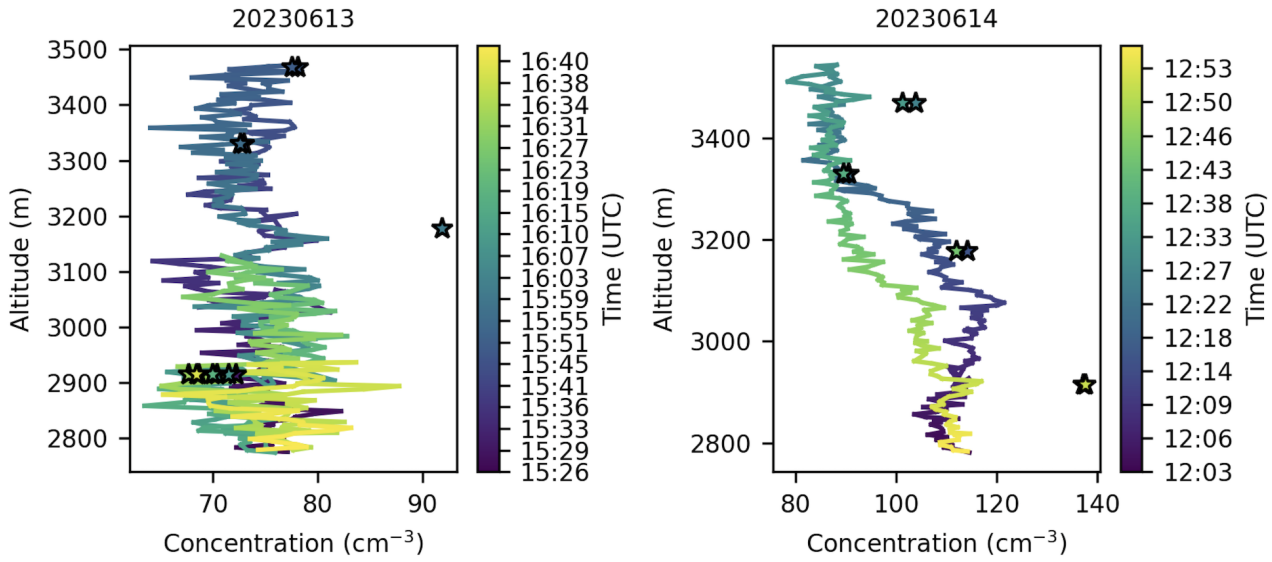

Figure 13. A visual comparison between the TBS flight on 13 and 14 June 2023 and the pseudo vertical column generated by the SAIL-Net sites. Each star marks one of the measurements in SAIL-Net's pseudo vertical column, plotted at the altitude above sea level of the site. There is one star for every time the altitude above sea level of the TBS flight passed within 2.5 m of the altitude of the SAIL-Net site.

2024, the column of air was not as vertically mixed. Though not displayed here, some flights also passed through plumes at certain altitudes where concentrations momentarily spiked.

For each flight, we computed both the absolute value of the percent difference between the vertical column of the flight and the vertical column of the sites, and the absolute difference between the two. This choice was made because the seasonality of total concentrations could make the percent error a less useful metric for understanding the differences in the region over time, as we saw in previous analysis. We grouped the errors together by day, even if there were multiple flights in a single day. Figure 14 plots a box plot of the absolute errors collected each day of flights as well as a line plot of the median percent error each day. While the TBS flew on more days than what is plotted below, we limited the comparison to days that the SAIL-Net vertical column was generated by at least half the SAIL-Net sites. We chose the median because we wanted to obtain a metric that represented the typical difference between the site and vertical column, and did not want to be influenced by outliers which were sometimes present, typically due to local sources at the ground-based sites. The median percent error between the two vertical columns was highest in April 2023, which is not surprising given that April typically had lower total aerosol concentrations than any of the warmer months in which balloons flew. The lowest median percent error of 4.7% occurred on 13 June 2023 and the highest error of 204.3% happened on 06 April 2023. 13 June 2024 also had a low absolute difference with a median concentration difference of 3.5 cm^{-3} and range of 15.4 cm^{-3}. By contrast, 06 April 2023 has a median concentration difference of 51.5 cm^{-3}, indicating that despite there being lower total aerosol concentrations in the spring, there was still a

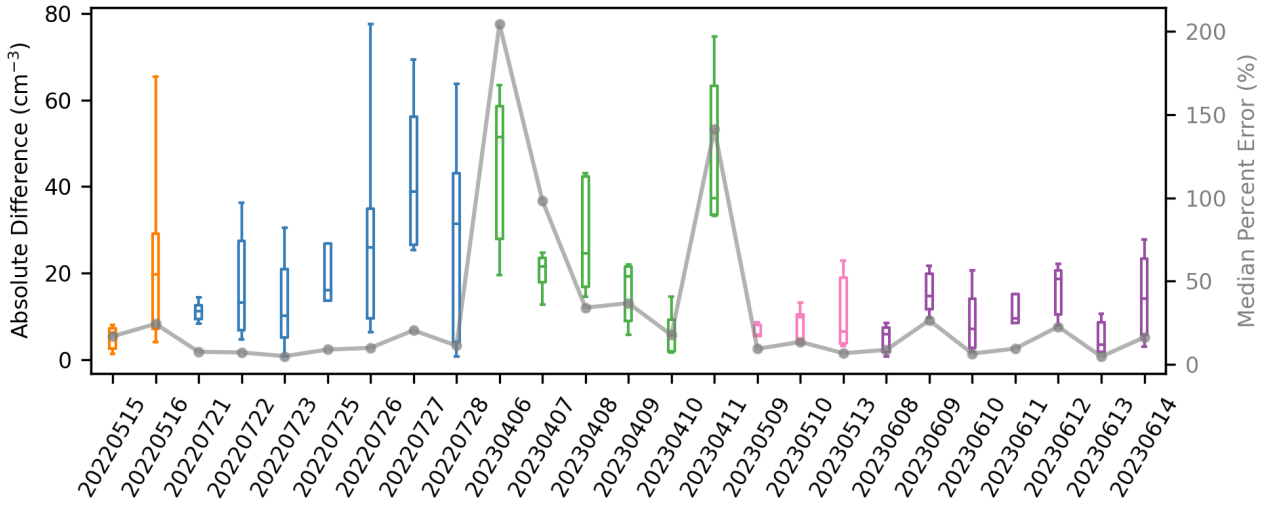

Figure 14. The daily absolute differences between the TBS vertical column and the SAIL-Net pseudo vertical column are plotted as box plots, where the interquartile range is given by the box and the whiskers extend to the 5th and 95th percentiles. The box plots have different colors based on which month the flight occurred. The median percent error is plotted as a gray line. Each date of the flight is mark on the x-axis in the form YYYYMMDD.

significant difference between the absolute measurements as well. Over 75% of the days had a median percent error under 25% and more than half the days had a median percent error below 15%.

Given the difference between these measurements – a true vertical column generated by airborne measurements compared to the pseudo vertical columns from ground-based measurements – these errors were surprisingly low. This suggests that the SAIL-Net sites were able to capture the vertical profile of aerosol decently well given the sample set. However, the majority of comparison days came from the spring and summer when there was more total aerosol and temperatures were warmer. During these days, there was likely in general better mixing of the boundary layer than there would be in the winter, meaning there was less vertical variability of air overall, as we see on 13 June 2023 in Figure 14. There would need to be significantly more comparisons such as this during different seasons and times of day to determine if dispersed, ground-based measurements at different elevations could sufficiently characterize the vertical column of air. These results do however further emphasize the relationship between aerosol variability and elevation in complex terrain.

4 Conclusions

SAIL-Net was the first of its kind in mountainous terrain and now presents a complete dataset highlighting the spatiotemporal variability of PM2.5 in complex terrain. The results of the above analysis indicate that there is some variability between the SAIL-Net sites, which appear to be at least partially driven by the elevation of sites. However, the differences between the sites

may not be significant enough depending on the measurements and use cases of them. This conclusion would ultimately be left to the user of the data.

SAIL-Net observed seasonal and diurnal cycles in aerosol concentrations. The highest concentrations occurred in late summer, but supermicron concentrations peaked in the spring, likely due to aeolian dust. Diurnal cycles were more pronounced in warmer months, agreeing with the findings of Gallagher et al. (2011). There was more variability between the sites in the winters than in the summers, possibly because the lower concentrations in the winters caused sites to be more sensitive to local sources. There is also a possibility that the winter time convective boundary layer was low enough that some higher elevation SAIL-Net sites were above it, also leading to increased variability, but more work should be done here to identify the cause.

The differences in concentration between the sites were partially related to their elevations, with a Pearson R-value of 0.44 relating elevation proximity to measurement similarity. This relationship between concentration and elevation was further supported by the ability of the sites to represent the vertical profile of air in the region. From the comparisons between site data and TBS flights, the error in the sites representing the vertical profile of air in the region was as low as 4.7% in June 2023. However, a spring day also measured an error as high as 204%, indicating that there was more than elevation that drove the variability between sites. The variability between sites was inconsistent over different seasons, underscoring the potential inadequacy of a single site to consistently represent the complex terrain in the ERW. However, the similar daily trends across the sites indicate that on a larger timescale, there is minimal variability in the region. Compared to the range of representation errors seen by Asher et al. (2022), SAIL-Net sites did experience larger representation errors over a smaller spatial region. This result emphasizes that there is increased variability of aerosol in complex terrain and also supports the findings from Zieger et al. (2012) in the Swiss Alps.

There is future work that could be done with this dataset. While this manuscript focused on the analysis of the variability and trends of the data, there are opportunities for modeling and further analysis. One such direction would be combining these data with other observations to begin to explain the behaviors observed here. For example, one could explore the possible causes of increased variability in the winter. Another direction would be exploring the diurnal cycles in aerosol concentrations to understand why concentrations decrease in the afternoons. Including data from new particle formation and studying the patterns in daily upslope and downslope winds may provide additional clarity. The comparison of the sites against measurements from tethered balloon flights in the region were surprisingly similar, and could warrant further investigation to learn a network of ground-based sensors in complex terrain could sufficiently characterize the vertical column of air in the region.

One of the primary drawbacks of these data was the gaps in data and possible remaining instrument differences. The gaps in data made it impossible to consistently compute a daily representation error from all six sites. This could affect the results of the representation and network analysis since the daily representation error was computed from the sites that did have data each day. However, we believe these possible errors do not affect the overall seasonal trends and the relationship between concentrations and elevations that we observed. While the data were post-corrected using monthly PSL checks, there may not have been frequent enough checks to correct all errors and drift. For example, unlike POPSnet, where two POPS were colocated to monitor accuracy, only one POPS was stationed at each site. However, we are still confident that the behavior observed at individual sites and between sites was predominately attributed to true measurements and not instrument differences.

This initial analysis supports the claim that aerosol concentrations are more variable both spatially and temporally in regions of complex terrain than in flat land. However, the similar trends in the data from daily averages in Fig. 4 do indicate that there is consistency across the region on a daily or larger timescale. This suggests that depending on the desired accuracy of modeling efforts in the region, it may be necessary to take this variability into account. Furthermore, the change in variability across seasons suggests that models may not retain the same accuracy over time. These data provide valuable insight into the variability of aerosol in mountainous terrain and serve as a blueprint for future measurement networks in similar regions.

Code and data availability. The datasets used in this analysis are available on Zenodo: https://doi.org/10.5281/zenodo.12747225. These datasets, as well as the raw data from the POPS areavailable on the ARM Data Discovery: https://doi.org/10.5439/2203692.

The code to perform all analysis and generate figures is located in a GitHub repository: https://zenodo.org/doi/10.5281/zenodo.11238718.

Author contributions. LG performed the data curation and formal analysis and wrote the manuscript. EL was the PI, led project administration, assisted with site setup and monthly visits, supervised data analysis, and provided writing review and editing support. EE helped with site identification and setup and performed monthly site visits. NG designed and set up sampling site infrastructure and assisted with monthly site visits. AH was the Co-PI, assisted with site setup and monthly site visits, and provided project supervision and management. GM was the Co-I, assisted with site setup and monthly site visits, and advised on project management and data analysis. KP assisted with site setup and monthly site visits. BR assisted with site setup and monthly site visits and advised on data analysis TR designed and built instrument enclosures. BS built CloudPucks and assisted with monthly site visits.

Competing interests. There are no competing interests.

Acknowledgements. We thank the US Department of Energy (DOE) Atmospheric System Research (ASR) program for funding through project DE-SC0022008. We thank Lawrence Berkeley National Laboratory (LBNL) for in-kind support. In-kind assistance from the LBNL was supported by the DOE Office of Science, Office of Biological and Environmental Research and Environmental System Science under DOE contract DE-AC02-05CH11231. We thank the Rocky Mountain Biological Laboratory (RMBL) for the use of their land for our Gothic site.

References

Adler, B., Wilczak, J. M., Bianco, L., Bariteau, L., Cox, C. J., De Boer, G., Djalalova, I. V., Gallagher, M. R., Intrieri, J. M., Meyers, T. P., Myers, T. A., Olson, J. B., Pezoa, S., Sedlar, J., Smith, E., Turner, D. D., and White, A. B.: Impact of Seasonal Snow-Cover Change on the Observed and Simulated State of the Atmospheric Boundary Layer in a High-Altitude Mountain Valley, Journal of Geophysical Research: Atmospheres, 128, e2023JD038 497, https://doi.org/10.1029/2023JD038497, 2023.

Anderson, T. L., Charlson, R. J., Winker, D. M., Ogren, J. A., and Holmén, K.: Mesoscale Variations of Tropospheric Aerosols*, Journal of the Atmospheric Sciences, 60, 119–136, https://doi.org/10.1175/1520-0469(2003)060<0119:MVOTA>2.0.CO;2, 2003.

Asher, E., Thornberry, T., Fahey, D. W., McComiskey, A., Carslaw, K., Grunau, S., Chang, K.-L., Telg, H., Chen, P., and Gao, R.-S.: A Novel Network-Based Approach to Determining Measurement Representation Error for Model Evaluation of Aerosol Microphysical Properties, Journal of Geophysical Research: Atmospheres, 127, https://doi.org/10.1029/2021JD035485, 2022.

Brus, D., Gustafsson, J., Vakkari, V., Kemppinen, O., De Boer, G., and Hirsikko, A.: Measurement Report: Properties of Aerosol and Gases in the Vertical Profile during the LAPSE-RATE Campaign, Atmospheric Chemistry and Physics, 21, 517–533, https://doi.org/10.5194/acp-21-517-2021, 2021.

Caubel, J. J., Cados, T. E., Preble, C. V., and Kirchstetter, T. W.: A Distributed Network of 100 Black Carbon Sensors for 100 Days of Air Quality Monitoring in West Oakland, California, Environmental Science & Technology, 53, 7564–7573, https://doi.org/10.1021/acs.est.9b00282, 2019.

Creamean, J. M., Suski, K. J., Rosenfeld, D., Cazorla, A., DeMott, P. J., Sullivan, R. C., White, A. B., Ralph, F. M., Minnis, P., Comstock, J. M., Tomlinson, J. M., and Prather, K. A.: Dust and Biological Aerosols from the Sahara and Asia Influence Precipitation in the Western U.S., Science, 339, 1572–1578, https://doi.org/10.1126/science.1227279, 2013.

Creamean, J. M., Primm, K. M., Tolbert, M. A., Hall, E. G., Wendell, J., Jordan, A., Sheridan, P. J., Smith, J., and Schnell, R. C.: HOVERCAT: A Novel Aerial System for Evaluation of Aerosol–Cloud Interactions, Atmospheric Measurement Techniques, 11, 3969–3985, https://doi.org/10.5194/amt-11-3969-2018, 2018.

Feldman, D., Aiken, A., Boos, W. R., Carroll, R., Chandrasekar, V., Collis, S., Creamean, J. M., De Boer, G., Deems, J., DeMott, P. J., Fan, J., Flores, A. N., Gochis, D., Grover, M., Hill, T. C. J., Hodshire, A., Hulm, E., Hume, C. C., Jackson, R., Junyent, F., Kennedy, A., Kumjian, M., Levin, E. J. T., Lundquist, J. D., O'Brien, J., Raleigh, M. S., Reithel, J., Rhoades, A., Rittger, K., Rudisill, W., Sherman, Z., Siirila-Woodburn, E., Skiles, S. M., Smith, J. N., Sullivan, R. C., Theisen, A., Tuftedal, M., Varble, A. C., Wiedlea, A., Wielandt, S., Williams, K., and Xu, Z.: The Surface Atmosphere Integrated Field Laboratory (SAIL) Campaign, Bulletin of the American Meteorological Society, https://doi.org/10.1175/BAMS-D-22-0049.1, 2023.

Gallagher, J. P., McKendry, I. G., Macdonald, A. M., and Leaitch, W. R.: Seasonal and Diurnal Variations in Aerosol Concentration on Whistler Mountain: Boundary Layer Influence and Synoptic-Scale Controls, Journal of Applied Meteorology and Climatology, 50, 2210–2222, https://doi.org/10.1175/JAMC-D-11-028.1, 2011.

Gao, R. S., Telg, H., McLaughlin, R. J., Ciciora, S. J., Watts, L. A., Richardson, M. S., Schwarz, J. P., Perring, A. E., Thornberry, T. D., Rollins, A. W., Markovic, M. Z., Bates, T. S., Johnson, J. E., and Fahey, D. W.: A Light-Weight, High-Sensitivity Particle Spectrometer for PM2.5 Aerosol Measurements, Aerosol Science and Technology, 50, 88–99, https://doi.org/10.1080/02786826.2015.1131809, 2016.

Gibson, L. and Levin, E.: SAIL-Net Raw and Post Corrected POPS Data Fall 2021 - Summer 2023, https://doi.org/10.5439/2203692, 2023.

Jha, V., Cotton, W. R., Carrió, G. G., and Walko, R.: Seasonal Estimates of the Impacts of Aerosol and Dust Pollution on Orographic Precipitation in the Colorado River Basin, Physical Geography, 42, 73–97, https://doi.org/10.1080/02723646.2020.1792602, 2021.

Jirak, I. L. and Cotton, W. R.: Effect of Air Pollution on Precipitation along the Front Range of the Rocky Mountains, Journal of Applied Meteorology and Climatology, 45, 236–245, https://doi.org/10.1175/JAM2328.1, 2006.

Kelly, K. E., Xing, W. W., Sayahi, T., Mitchell, L., Becnel, T., Gaillardon, P.-E., Meyer, M., and Whitaker, R. T.: Community-Based Measurements Reveal Unseen Differences during Air Pollution Episodes, Environmental Science & Technology, 55, 120–128, https://doi.org/10.1021/acs.est.0c02341, 2021.

Levin, E. J., DeMott, P. J., Suski, K. J., Boose, Y., Hill, T. C., McCluskey, C. S., Schill, G. P., Rocci, K., Al-Mashat, H., Kristensen, L. J., Cornwell, G., Prather, K., Tomlinson, J., Mei, F., Hubbe, J., Pekour, M., Sullivan, R., Leung, L. R., and Kreidenweis, S. M.: Characteristics of Ice Nucleating Particles in and Around California Winter Storms, Journal of Geophysical Research: Atmospheres, 124, 11 530–11 551, https://doi.org/10.1029/2019JD030831, 2019.

Lynn, B., Khain, A., Rosenfeld, D., and Woodley, W. L.: Effects of Aerosols on Precipitation from Orographic Clouds: EFFECTS OF AEROSOLS ON PRECIPITATION, Journal of Geophysical Research: Atmospheres, 112, https://doi.org/10.1029/2006JD007537, 2007.

Maupin, M. A., Ivahnenko, T. I., and Bruce, B.: Estimates of water use and trends in the Colorado River Basin, Southwestern United States, 1985–2010, Scientific Investigations Report, https://doi.org/10.3133/sir20185049, 2018.

Mei, F., McMeeking, G., Pekour, M., Gao, R.-S., Kulkarni, G., China, S., Telg, H., Dexheimer, D., Tomlinson, J., and Schmid, B.: Performance Assessment of Portable Optical Particle Spectrometer (POPS), Sensors, 20, 6294, https://doi.org/10.3390/s20216294, 2020.

Mei, F., Stephenson, J., and Pekour, M.: portable optical particle spectrometer aboard an airborne platform (TBSPOPS), https://doi.org/10.5439/1827703, 2023.

Nakata, M., Kajino, M., and Sato, Y.: Effects of Mountains on Aerosols Determined by AERONET/DRAGON/J-ALPS Measurements and Regional Model Simulations, Earth and Space Science, 8, e2021EA001 972, https://doi.org/10.1029/2021EA001972, 2021.

NRCS: Snow Water Equivalent in Gunnison, https://nwcc-apps.sc.egov.usda.gov/awdb/basin-plots/POR/WTEQ/assocHUCco_8/gunnison.html, 2023.

Perkins, R., DeMott, P., Kreidenweis, S., Levin, E., and Hodshire, A.: Vertical Aerosol Profiling during SAIL (VAPS) Field Campaign Report, https://doi.org/10.2172/1974540, 2023.

Popoola, O. A., Carruthers, D., Lad, C., Bright, V. B., Mead, M. I., Stettler, M. E., Saffell, J. R., and Jones, R. L.: Use of Networks of Low Cost Air Quality Sensors to Quantify Air Quality in Urban Settings, Atmospheric Environment, 194, 58–70, https://doi.org/10.1016/j.atmosenv.2018.09.030, 2018.

Rosenfeld, D., Andreae, M. O., Asmi, A., Chin, M., de Leeuw, G., Donovan, D. P., Kahn, R., Kinne, S., Kivekäs, N., Kulmala, M., Lau, W., Schmidt, K. S., Suni, T., Wagner, T., Wild, M., and Quaas, J.: Global Observations of Aerosol-Cloud-Precipitation-Climate Interactions: Aerosol-cloud-climate Interactions, Reviews of Geophysics, 52, 750–808, https://doi.org/10.1002/2013RG000441, 2014.

Saleeby, S. M., Cotton, W. R., and Fuller, J. D.: The Cumulative Impact of Cloud Droplet Nucleating Aerosols on Orographic Snowfall in Colorado, Journal of Applied Meteorology and Climatology, 50, 604–625, https://doi.org/10.1175/2010JAMC2594.1, 2011.

Schneider, P., Castell, N., Vogt, M., Dauge, F. R., Lahoz, W. A., and Bartonova, A.: Mapping Urban Air Quality in near Real-Time Using Observations from Low-Cost Sensors and Model Information, Environment International, 106, 234–247, https://doi.org/10.1016/j.envint.2017.05.005, 2017.

Schutgens, N., Tsyro, S., Gryspeerdt, E., Goto, D., Weigum, N., Schulz, M., and Stier, P.: On the Spatio-Temporal Representativeness of Observations, Atmospheric Chemistry and Physics, 17, 9761–9780, https://doi.org/10.5194/acp-17-9761-2017, 2017.

Schutgens, N. A. J., Gryspeerdt, E., Weigum, N., Tsyro, S., Goto, D., Schulz, M., and Stier, P.: Will a Perfect Model Agree with Perfect Observations? The Impact of Spatial Sampling, Atmospheric Chemistry and Physics, 16, 6335–6353, https://doi.org/10.5194/acp-16-6335-2016, 2016.

Skiles, S. M., Painter, T. H., Belnap, J., Holland, L., Reynolds, R. L., Goldstein, H. L., and Lin, J.: Regional Variability in Dust-on-snow Processes and Impacts in the Upper Colorado River Basin, Hydrological Processes, 29, 5397–5413, https://doi.org/10.1002/hyp.10569, 2015.

Todt, M. A., Asher, E., Hall, E., Cullis, P., Jordan, A., Xiong, K., Hurst, D. F., and Thornberry, T.: Baseline Balloon Stratospheric Aerosol Profiles (B ^{2} SAP)—Systematic Measurements of Aerosol Number Density and Size, Journal of Geophysical Research: Atmospheres, 128, e2022JD038 041, https://doi.org/10.1029/2022JD038041, 2023.

Weigum, N., Schutgens, N., and Stier, P.: Effect of Aerosol Subgrid Variability on Aerosol Optical Depth and Cloud Condensation Nuclei: Implications for Global Aerosol Modelling, Atmospheric Chemistry and Physics, 16, 13 619–13 639, https://doi.org/10.5194/acp-16-13619-2016, 2016.

Yuan, Q., Wan, X., Cong, Z., Li, M., Liu, L., Shu, S., Liu, R., Xu, L., Zhang, J., Ding, X., and Li, W.: In Situ Observations of Light-Absorbing Carbonaceous Aerosols at Himalaya: Analysis of the South Asian Sources and Trans-Himalayan Valleys Transport Pathways, Journal of Geophysical Research: Atmospheres, 125, e2020JD032 615, https://doi.org/10.1029/2020JD032615, 2020.

Zieger, P., Kienast-Sjögren, E., Starace, M., von Bismarck, J., Bukowiecki, N., Baltensperger, U., Wienhold, F. G., Peter, T., Ruhtz, T., Collaud Coen, M., Vuilleumier, L., Maier, O., Emili, E., Popp, C., and Weingartner, E.: Spatial Variation of Aerosol Optical Properties around the High-Alpine Site Jungfraujoch (3580 m a.s.l.), Atmospheric Chemistry and Physics, 12, 7231–7249, https://doi.org/10.5194/acp-12-7231-2012, 2012.